Targeting SARS-CoV-2 receptor-binding domain to cells expressing CD40 improves protection to infection in convalescent macaques

Romain Marlin
CEA https://orcid.org/0000-0001-8932-0171
Véronique Godot
INSERM, VRI
Sylvain Cardinaud
INSERM, VRI
Mathilde Galhaut
Université Paris-Saclay, INSERM, CEA
Severin Coleon
INSERM, VRI
Sandra Zurawski
Baylor Scott and White Research Institute
Nathalie Dereuddre-Bosquet
CEA https://orcid.org/0000-0001-6682-6313
Mariangela Cavarelli
Université Paris-Saclay, INSERM, CEA https://orcid.org/0000-0002-8468-0263
Anne-Sophie Gallouet
CEA/UMR 967
Mélanie Prague
Univ. Bordeaux, Department of Public Health, Inserm Bordeaux Population Health Research Centre
Pauline Maisonnasse
CEA - Université Paris Saclay - INSERM U1184 https://orcid.org/0000-0002-0555-207X
Léa Dupaty
INSERM, VRI
Craig Fenwick
Service of Immunology and Allergy, Lausanne University Hospital, University of Lausanne
Thibaut Naninck
CEA – Université Paris Saclay – INSERM U1184
Julien Lemaitre
CEA – Université Paris Saclay – INSERM U1184
Mario Gomez-Pacheco

Université Paris-Saclay, INSERM, CEA

Nidhal Kahlaoui

Université Paris-Saclay, Inserm, CEA, Center for Immunology of Viral, Auto-immune, Hematological and Bacterial diseases

Vanessa Contreras

CEA - Université Paris Saclay - INSERM U1184

Francis Relouzat

CEA

Raphael Ho Tsong Fang

CEA – Université Paris Saclay – INSERM U1184

Zhiqing Wang

Baylor Scott and White Research Institute

Jerome Ellis III

Baylor Scott and White Research Institute

Catherine Chapon

CEA – Université Paris Saclay – INSERM U1184

Mireille Centlivre

INSERM, VRI https://orcid.org/0000-0001-7616-9775

Inga Szurgot

Department of Microbiology, Tumor and Cell Biology, Karolinska Institutet

Peter Liljeström

Department of Microbiology, Tumor and Cell Biology, Karolinska Institutet

Sylvie van der Werf

Institut Pasteur https://orcid.org/0000-0002-1148-4456

Giuseppe Pantaleo

University Hospital of Lausanne

Rodolphe Thiébaut

Univ. Bordeaux, Department of Public Health, Inserm Bordeaux Population Health Research Centre https://orcid.org/0000-0002-5235-3962

Gerard Zurawski

Baylor Scott and White Research Institute

Yves Levy

Vaccine Research Institute https://orcid.org/0000-0002-5549-6256

Roger Le Grand (roger.le-grand@cea.fr)

Université Paris-Saclay, INSERM, CEA https://orcid.org/0000-0002-4928-4484

Article

Keywords: Vaccine, SARS-CoV-2, DC-targeting, convalescent, Non-Human Primate

Posted Date: February 19th, 2021

DOI: https://doi.org/10.21203/rs.3.rs-244682/v1

Version of Record: A version of this preprint was published at Nature Communications on September 1st, 2021. See the published version at https://doi.org/10.1038/s41467-021-25382-0.

Abstract

Controlling the circulation of the recently emerged SARS-CoV-2 in the human populations requires massive vaccination campaigns. Achieving sufficient worldwide vaccination coverage will require additional approaches to first generation of approved viral vector and mRNA vaccines. Subunit vaccines have excellent safety and efficacy records and may have distinct advantages, in particular when immunizing individuals with vulnerabilities or when considering the vaccination of children and pregnant women. We have developed a new generation of subunit vaccines with enhanced immunogenicity by the targeting of viral antigens to CD40-expressing antigen-presenting cells, thus harnessing their intrinsic immune-stimulant properties. Here, we demonstrate that targeting the receptor-binding domain (RBD) of the SARS-CoV-2 spike protein to CD40 (αCD40.RBD) induces significant levels of specific T and B cells, with a long-term memory phenotype, in a humanized mouse model. In addition, we demonstrate that a single dose of the αCD40.RBD vaccine, injected without adjuvant, is sufficient to boost a rapid increase in neutralizing antibodies in convalescent non-human primates (NHPs) exposed six months previously to SARS-CoV-2. Such vaccination thus significantly improved protection against a new high-dose virulent challenge versus that in non-vaccinated convalescent animals. Viral dynamics modelling showed the high efficiency of the vaccine at controlling the viral dissemination.

Main Text

Coronavirus-induced disease 2019 (COVID-19) is caused by a zoonotic virus, severe acute respiratory syndrome coronavirus 2 (SARS-CoV-2), which has rapidly spread during the last year and a half, infecting over 100 million humans and causing more than two million deaths worldwide. Durable control of the pandemic requires mass vaccination strategies, for which the first vaccine candidates became available at the end of 2020. Although there are a limited number of previously licensed vector-based vaccines for human use, recombinant DNA vector and synthetic mRNA vaccines have nevertheless become the most advanced in the fight against COVID-19 because of the many possibilities offered for genetic engineering and rapid scalability [1-4]. Given that the benefits outweigh the risks for their use in humans, an Emergency Use Authorization (EUA) was favorably evaluated by the US Food and Drug Administration (FDA) for the first two mRNA vaccines encoding a pre-fusion stabilized SARS-CoV-2 spike glycoprotein [3,5-7]. The estimated efficacy after phase III clinical trial interim analysis was approximately 94% to 95% in preventing COVID-19 in the short term following the second immunization. Continued evaluation of the effectiveness of the vaccines following EUA issuance is needed to confirm these initial promising results. Long-term efficacy data will be critical for estimating their impact on progression of the pandemic. Initial reports on adverse events may not limit their deployment, but safety assessments require extended follow-up. Further evaluations will also be needed to assess the efficacy of the vaccines in preventing asymptomatic infections and reducing viral shedding to the level required to prevent secondary transmission. If not efficiently prevented, asymptomatic infections in combination with reduced mask wearing and social distancing could result in significant continuing circulation of the virus [5].

A new generation of COVID-19 vaccines is needed to counteract the development of the pandemic. Providing the necessary billions of doses to achieve sufficient global coverage will not be possible with any single product. In addition, there are uncertainties about the long-term efficacy and safety of these first-in-class vector or mRNA vaccine platforms, with a limited history of use, particularly in vulnerable individuals, including frail, older individuals, people with co-morbidities, and immunosuppressed patients. Importantly, the use of vector-based vaccines will require cautious and long-term safety assessment before considering their use in children and pregnant women. Although younger individuals are less prone to develop severe disease, they are susceptible to mild COVID-19 or asymptomatic infection and may facilitate circulation of the virus and the potential for further mutation. Control of the pandemic will also require the mass immunization of children.

The constraints of antigen design and engineering and the time required for the production of large numbers of doses make subunit vaccines difficult to develop as first countermeasures for suddenly emerging and non-anticipated epidemics. However, licensed subunit vaccines have proven tolerability and safety in diverse population classes [8]. Several adjuvanted SARS-CoV-2 spike protein vaccines are able to elicit neutralizing antibodies to protective levels in relevant animal models, including non-human primate (NHP) challenge studies [9-11]. These advantages may be decisive in the development of the next-generation vaccines aimed at controlling the long-term circulation of SARS-CoV-2, in particular if the virus continues provoking seasonal epidemic waves of COVID-19.

Dendritic cells (DCs) are immune system controllers that can deliver differential signals to other immune cells through intercellular interactions and soluble factors, resulting in a variety of host immune responses of varying quality. Targeting vaccine antigens to DCs via surface receptors represents an appealing strategy to improve subunit-vaccine efficacy while reducing the amount of required antigen. Direct delivery of the antigen, which can additionally activate cell receptors, may also evoke a danger signal, stimulating an immune response without the need of additional immune stimulants, such as adjuvants. Among the various DC receptors tested, including lectins and scavenger receptors, we reported the superiority of vaccines targeting diverse viral antigens to CD40 expressing antigen-presenting cells in evoking strong antigen-specific T- and B-cell responses [12-16]. Drawing from this knowledge, we developed a vaccine that targets the receptor-binding domain (RBD) of the SARS-CoV-2 spike antigen to the CD40 receptor (αCD40.RBD). We proved its immunogenicity in two different animal models. A single dose of the αCD40.RBD administered without adjuvant boosted the protective response in COVID-19 convalescent NHPs.

Humanized anti-CD40 monoclonal antibody fused to the receptor-binding domain of the spike antigen targets and activates human and macaque antigen-presenting cells

The human ACE2 receptor is the crucial target for the receptor-binding domain (RBD) of the spike (S) protein of SARS-CoV2, for which this strong interactive synapse assists viral entry into host cells [17]. The RBD is a logical target for the development of neutralizing antibodies, as well as serving as a potential source of T-cell epitopes to elicit cellular immune responses. Thus, we engineered vectors expressing

SARS-CoV-2 RBD (residues 173-591 of sequence ID: QIC50514.1) fused to the C-termini of the anti-human CD40 humanized 12E12 IgG4 antibody to generate the αCD40.RBD vaccine [16,18,19].

As evaluated by a solid-phase direct-binding assay [16], there was no significant difference in CD40 binding affinity (EC50 30 pM) between the 12E12 anti-CD40 monoclonal antibody (mAb) and 12E12 anti-CD40 fused to RBD (EC50 35 pM) (Fig. 1A and Extended data Fig. 1A). We have previously shown that 12E12 anti-CD40 fused to viral antigens enhances CD40-mediated internalization and antigen-presentation by mononuclear cells and *ex vivo* generated monocyte-derived DCs [12,18]. Similarly, we show here that the αCD40-RBD vaccine binds (Fig. 1B; Extended data Fig. 1B-C) and activates (Fig. 1C; Extended data Fig. 1D) macaque monocytes, DCs, and B cells obtained from peripheral blood mononuclear cells (PBMCs).

The αCD40-RBD vaccine induces robust human B- and T-cell responses in humanized mice

We first assessed the immunogenicity of the aCD40-RBD vaccine in NSG (NOD/SCID $gc^{-/-}$) mice with a human immune system (hu-mice) generated by reconstituting newborns with human fetal liver hematopoietic stem cells (Fig. 1D). A single injection of αCD40-RBD (10 µg) adjuvanted with polyinosinic-polycytidylic acid (Poly-IC, 50 µg) by the intraperitoneal route was sufficient to elicit SARS-CoV-2 S protein-specific IgG-switched human B cells in the blood of 50% of immunized mice (Fig. 1E). At week 6, one week after the last αCD40.RBD boost, unbiased t-SNE analysis of the splenic human $CD19^+$ B cells revealed cell clusters corresponding to well-described subsets of terminally differentiated plasma cells (PCs), early plasma blasts (PBs), and a contingent of PBs and immature PCs in the vaccine groups but not controls (Fig. 1F-I). At the same timepoint, splenic SARS-CoV-2 S protein-specific IgG-switched human B cells were detected in all vaccinated hu-mice (Fig. 1H), mainly of the PB and immature PC phenotype (Fig. 1H). All spike protein-specific IgG-switched human B cells expressed CXCR4 and a discrete cell island was observed in the t-SNE analysis driven by high expression of CCR10 (Fig. 1J), which was confirmed using manual back gating (Extended data Fig. 2A). We next evaluated the capacity of the vaccines to induce specific and functional $CD4^+$ and $CD8^+$ memory T cells. Th1 (IFN-$\gamma^{+/-}$ IL-$2^{+/-}$ TNF-α) type $CD4^+$ T-cell responses and IFNg-secreting $CD8^+$ T-cells were observed for the vaccinated hu-mice following *ex vivo* stimulation of splenocytes with RBD peptide pools (Extended data Fig. 2B-C). We confirmed the presence of human $CD8^+$ T cells specific for the predicted optimal epitopes from SARS-CoV-2 RBD protein in the spleens of vaccinated hu-mice using HLA-I tetramers (Extended data Fig. 2D-E).

Subunit vaccines could also be considered as boosters for other type of vaccines in human vaccination campaigns. Thus, in addition to a homologous prime-boost regime, we tested the capacity of αCD40.RBD to boost heterologous priming with a vector-based vaccine. The DNA-launched self-amplifying RNA replicon vector encoding the SARS-CoV-2 spike glycoprotein (DREP)-S is a previously described platform [20] based on the alphavirus genome encoding the genes for the viral RNA replicase but lacking those encoding the structural proteins of the virus [21]. We demonstrated that αCD40.RBD efficiently boosted (DREP)-S primed B- and T-cell SARS-CoV-2 specific responses (Fig. 1E, 1I; Extended data Fig. 2).

The αCD40.RBD vaccine recalls specific immune responses in convalescent macaques

The results in the hu-mice model are consistent with those of our previous CD40-targeted influenza and HIV vaccine studies [13,14,18,19] and demonstrate that αCD40.RBD is a potent prime or boost vaccine for eliciting RBD-specific T- and B-cell responses similar in magnitude to previously reported protective responses [11]. In addition, we previously showed that nanomolar amounts of αCD40 vaccines can elicit *in vitro* recall responses in PBMCs collected from individuals primed by the natural viral infection [18,22]. Thus, we tested the hypothesis that the αCD40.RBD vaccine can efficiently elicit recall responses *in vivo* in SARS-CoV-2 convalescent individuals. The improved immunogenicity obtained by CD40 targeting and the stimulating capacity of the αCD40.RBD vaccine also suggested that adjuvant may not be necessary to elicit a protective recall response. We thus subcutaneously injected six convalescent cynomolgus macaques with 200 µg of the vaccine without adjuvant. An additional 12 animals (six convalescent and six naive) were injected with PBS as controls (Fig. 2A). All the convalescent macaques, randomly distributed between the vaccine and control groups, had been infected approximately six months before this study (range = 26-24 weeks) with SARS-CoV-2 in a study to evaluate pre-exposure or post-exposure prophylaxis with hydroxychloroquine (HCQ). No evidence of antiviral efficacy [23] of HCQ was observed and after this first exposure to the virus, all animals developed similar profiles of viral load (Extended data Fig. 3A and 3B) and suffered from transient and moderate disease, resulting in increased levels of anti-S IgG antibodies detected in the serum (Fig. 2B). At the time of the αCD40.RBD-vaccine injection, anti-S IgG levels in the two groups of convalescent macaques were comparable and in the average range of specific responses detected in the sera of convalescent patients (Fig. 2C). Before vaccination, the infection of macaques with SARS-CoV-2 generated both anti-RBD antibodies (Fig. 2D) and low but detectable levels of antibodies inhibiting the binding of the spike protein to the ACE2 receptor (Fig. 2E). Before vaccination, low Th1 (IFN-$\gamma^{+/-}$ IL-$2^{+/-}$ TNF-α) type $CD4^+$ T-cell responses were observed for both groups of convalescent macaques following *ex vivo* stimulation of PBMCs with RBD and N-peptide pools (Fig. 2F; Extended data Fig. 2E). None of the convalescent animals had detectable anti-RBD or anti-N $CD8^+$ T cells (Extended data Fig. 2F).

Two weeks after αCD40.RBD vaccine injection, all six vaccinated macaques exhibited significantly increased levels of anti-S (Fig. 2B) and anti-RBD IgG (Fig. 2D) in the serum, which correlated with an increased capacity of inhibition of RBD binding to the ACE2 receptor ($p = 0.022$, Fig. 2E), as they remained elevated four weeks after vaccination. None of these parameters increased in PBS-injected convalescent controls (Fig. 2D and 2E). In addition, anti-S IgG levels in the vaccinated macaques were higher ($p = 0.0018$) than those typically observed in humans 1 to 3 months after symptomatic SARS-CoV-2 infection (Extended data Fig. 3C). The immunization also elicited a significant increase in the anti-RBD Th1 response in all six immunized animals ($p = 0.031$; Fig. 2F-G), whereas no changes in the magnitude of anti-N $CD4^+$ T cells (Extended data Fig. 4E) or SARS-CoV-2 specific $CD8^+$ T cells was observed (Extended data Fig. 4F).

The αCD40.RBD vaccine improves the protection of convalescent macaques against SARS-CoV-2 reinfection

Four weeks following vaccine or placebo injection, the 12 convalescent macaques were exposed a second time to a high dose ($1x10^6$ pfu) of SARS-CoV-2 administered via the combined intra-nasal and intra-tracheal route using a previously reported challenge procedure [23]. Six SARS-CoV-2 naive animals were also challenged as controls.

All naive animals became infected, as shown by the detection of viral genomic (gRNA) and sub-genomic (sgRNA) RNA in tracheal (Fig. 3A-D; Extended data Fig. 5A and 5B) and nasopharyngeal (Fig. 3D; Extended data Fig. 5C-G) swabs and broncho-alveolar lavages (BAL, Fig. 3E and Extended data Fig. 5H). Of note, the dynamics of viral replication in these animals was comparable to that observed during the first infection six months earlier in the two groups of convalescent macaques (Extended data Fig. 3A-B). The non-vaccinated convalescent animals were not protected against the second SARS-CoV-2 challenge, but significantly lower viral RNA levels were detected in the upper respiratory tract than in the naive animals (Fig. 3A-E and Extended data Fig. 5). The αCD40.RBD vaccine remarkably improved the partial protection observed in the convalescent macaques. All vaccinated animals exhibited significantly lower viral gRNA levels ($p = 0.015$, Fig. 3D) than the non-vaccinated convalescent animals. The levels of sgRNA remained below the limit of detection in upper respiratory tract samples for 5 of 6 vaccinated animals, whereas sgRNA was detected in 4 of 6 non-vaccinated convalescent and all naive control animals (Extended data Fig. 5B and 5G). Moreover, the time post-exposure (p.expo.) to reach undetectable gRNA levels was significantly lower in vaccinated convalescent than non-vaccinated and control animals (Fig. 3C and Extended data Fig. 5E, log rank, $p < 0.0001$). The efficacy of vaccination was also higher in the lower respiratory tract, as only 3 of 6 vaccinated macaques were above the limit of detection for gRNA in BAL at day 3 p.expo. versus day 6 for the six non-vaccinated convalescent animals (Fig. 3E). Complete protection from shedding of the virus from the gastrointestinal tract was noted in the immunized macaques (Extended data Fig. 5I), which is probably an important factor to prevent secondary viral transmission [24].

The reduction of viral load in vaccinated and non-vaccinated convalescent macaques relative to naive infected animals was associated with a limited impact on leukocyte numbers (Extended data Fig. 6) and reduced cytokine concentrations in the plasma, in particular those of IL-1RA and CCL2 (Extended data Fig. 7B). Such viral loads and cytokine profiles were also associated with a reduction in lung lesions (Fig. 3H and Extended data Fig. 8), as scored by X-ray computerized tomography (CT).

We then analyzed the immune responses of all animals following SARS-CoV-2 viral challenge. The naive controls showed the slowest development of anti-S, anti-RBD, and anti-N IgG (Fig. 3F), of which the levels remained significantly lower than for the other two groups at day 20 p.expo. ($p = 0.022$). The non-vaccinated convalescent animals raised a rapid and robust anamnestic antibody response (Fig. 3F), which was associated with a significant increase ($p = 0.031$) in the serum capacity to neutralize ACE2 binding to RBD (Fig. 3G) by p.expo. day 9. The anti-S- and anti-RBD-specific antibody responses and neutralization activity of the serum was maintained in the vaccinated macaques at the high levels already achieved at the time of challenge and remained superior to that of the control macaques (Fig. 3F and 3G). The anti-RBD Th1 $CD4^+$ response increased post challenge for most of the control (convalescent

and naive) animals, with higher levels for some of the naive controls as early as p.expo. day 9 (Extended data Fig. 4G). On the contrary, all 18 animals showed comparable antibody and $CD4^+$ T cell responses to the N-peptide pool (Extended data Fig. 4G), probably reflecting a predominance of the response against non-structural antigens in infected individuals. The IFN-□-mediated $CD8^+$ T-cell response was also mainly directed against the N peptides (Extended data Fig. 4D), but with a significantly reduced intensity in all convalescent macaques than in the naive controls (Extended data Fig. 4H), probably reflecting the lower exposure to viral antigens as a result of better control of viral replication.

Spearman analysis between all recorded parameters revealed that the induction of anti-RBD- and ACE2-inhibiting antibodies was the strongest parameter to correlate with the reduction of viral load and disease markers, as were the plasma levels of the inflammatory cytokines IL-1RA and CCL2 (Fig. 3I and J).

Modeling of the dynamics of viral replication supports the capacity of αCD40.RBD to induce the blockade of initial viral entry into host cells and then limit secondary transmission

We developed a mathematical model to better characterize the impact of the immune response on viral gRNA and sgRNA dynamics. We wished to compare the differences in immunity, in particular in the reduction of the cell-infection rate and the increase in the clearance of infected cells generated by vaccination versus immunity developed after infection. The model was adapted from previously published studies [25,26] and includes uninfected target cells (T) that can be infected (I_1) and then produce virus after an eclipse phase (I_2). The virus generated can be infectious (V_I) or non-infectious (V_{NI}). We completed the model with a compartment for the inoculum to distinguish between the injected virus (V_s) and the virus produced *de novo* by the host (V_I and V_{NI}). We estimated viral infectivity (β) and the loss rate of infected cells (δ) using the sRNA and sgRNA viral loads, measuring V_S, V_I, and V_{NI}.

In this model, the αCD40.RBD vaccine reduced the infection of target cells in the trachea by an estimated 99% (Fig. 4, Table 1) relative to the two other groups, suggesting that the levels of anti-RBD antibodies induced by the vaccine are highly efficient for the neutralization of new infections *in vivo*. In addition, both specific antibodies and specific $CD8^+$ T cells are mechanisms commonly considered to be important for killing infected cells and thus reducing dissemination of the virus. According to our model, the estimated clearance of infected cells was 0.94 /day (95% CI 0.87; 1.02) in naive macaques, which was increased by 2.18-fold (118%) in the non-vaccinated convalescent and 2.86 fold in the αCD40.RBD-vaccinated convalescent animals (149% relative to naive controls and 31% relative to convalescent controls). Hence, the model predicts that the target cell levels (all infected and non-infected cells expressing ACE2) would be decreased by the previous infection in the naive and convalescent groups, whereas it would be preserved in vaccinated animals due to the blockade of new infections and increased clearance of infected cells. Similar effects were predicted for the nasopharyngeal compartment (Extended data Fig. 9).

Conclusions

In humans, the durability of protection induced by natural SARS-CoV-2 infection and the first vaccine candidates is unknown. In convalescent humans, the virus neutralizing-antibody response wanes and re-infections have been reported within months following previous exposure [24,27]. The decrease in neutralizing-antibody levels observed in most patients within three months post-infection may suggest that vaccine boosters will be required to provide long-lasting protection [28]. In contrast to previous NHP re-challenge studies performed shortly after a first infection [29], we demonstrate that SARS-CoV-2 reinfection is not fully prevented in convalescent macaques six months after initial exposure to the virus, confirming that protective immunity wanes over time. In addition, the vaccines currently used in humans are aimed at preventing severe disease and information is still lacking as to their capacity to prevent infection and reduce initial viral replication. Vaccinated individuals who develop an asymptomatic or mild symptomatic infection may continue transmitting the virus and actively contribute to circulation of the virus. The αCD40.RBD vaccine we developed significantly improved immunity when administered to convalescent macaques, resulting in a reduction of viral load following re-exposure to the virus down to levels that may avoid such secondary transmission. This vaccine may therefore represent an excellent booster of pre-existing immunity, either induced by natural infection or previous priming with vector-based vaccines. Indeed, we confirmed the efficacy of αCD40.RBD as a booster in (DREP)-S primed hu-mice. This new-generation subunit vaccine, improved by targeting of the antigen to CD40-expressing cells, may have decisive advantages for the rapid provision of a safe and efficient boosting strategy. The capacity to induce protective immunity without requiring an adjuvant would accelerate the development of a vaccine with improved tolerability for people with specific vulnerabilities and children, an important part of the population to consider in the control of circulation of the virus.

Methods

Ethics and biosafety statement animal studies

The NSG (NOD.Cg-Prkdcscid Il2rgtm1Wjl/SzJ) humanized mice (hu-mice) were supplied by the Jackson Laboratories (Bar Harbor, ME, USA) under MTA #1720. Five donors whose HLA typing is recapitulated in the supplemental table S1 provided hematopoietic stem cells for human immune system reconstitution of the mice. The level of human immune cells reconstitution reached an average of 70%. The hu-mice were housed in Mondor Institute of Biomedical Research infrastructure facilities (U955 INSERM-Paris East Creteil University, Ile-de-France, France). The protocols were approved by the institutional ethical committee “Comité d’Ethique Anses/ENVA/UPEC (CEEA-016)” under statement number 20-043 #25329. The study was authorized by the “Research, Innovation and Education Ministry” under registration number 25329-2020051119073072 v4.

Cynomolgus macaques (*Macaca fascicularis*), aged 37-58 months (8 females and 13 males) and originating from Mauritian AAALAC certified breeding centers were used in this study. All animals were housed in IDMIT facilities (CEA, Fontenay-aux-roses), under BSL-3 containment (Animal facility authorization #D92-032-02, Préfecture des Hauts de Seine, France) and in compliance with European Directive 2010/63/EU, the French regulations and the Standards for Human Care and Use of Laboratory

Animals, of the Office for Laboratory Animal Welfare (OLAW, assurance number #A5826-01, US). The protocols were approved by the institutional ethical committee “Comité d’Ethique en Expérimentation Animale du Commissariat à l’Energie Atomique et aux Energies Alternatives” (CEtEA #44) under statement number A20-011. The study was authorized by the “Research, Innovation and Education Ministry” under registration number APAFIS#24434-2020030216532863v1.

αCD40.RBD vaccine

Production and quality assurance of the αCD40.RBD vaccine Vectors and sequences for humanized anti-human CD40 12E12 IgG4 and control human IgG4 antibodies have been described previously [1,2,3]. GenBank sequences HQ738666.1 and KP684037 describe the human IgG4 chimeric forms of the 12E12, anti-human CD40 H and L chains. Methods for expression vectors and protein production and purification, via transient or stable CHO-S (Chinese Hamster Ovary cells) transfection and quality assurance including CD40 binding specificity were as are described. CHO-optimized codons encoding SARS-CoV-2 RBD residues 173-591 of sequence ID: QIC50514.1 with appended residues encoding a C-tag (EPEA) and a stop codon were inserted between the vector *Nhe* I and *Not* I sites positioned distal to the H chain C-terminal codon. Expression plasmids encoding the antibody H chain RBD fusion and the L chain were transiently transfected into Expi-CHO cells with TransIT-PRO Pro reagent (Mirus Bio) using the manufacturers protocol. The product was purified by protein A affinity capture of the culture medium followed by elution with a gradient of 1M L-Arginine monohydrochloride in H2O, from pH 8.0 and pH 1.8. Product was formulated in phosphate buffered saline (pH 7.4) with 125 mM cyclodextrin (average MW 1420). The LPS value was .037 ng/mg. Using a solid phase assay direct binding assay previously described [3] these was no significant difference in the CD40 binding affinity of anti-CD40 12E12 (EC50 30 pM) versus anti-CD40 12E12-RBD (EC50 35 pM).

DREP-S vaccine

DREP-S vaccine constructs were made by cloning the sequences encoding S of SARS-CoV-2 spike protein into the Semliki Forest Virus (SFV) DREP plasmid vector backbone 3 using BamHI and SpeI restriction sites [4]. The S construct encodes the surface glycoprotein of SARS-CoV-2 (Wuhan-Hu-1) with an 18-aa deletion in the cytoplasmic tail (D18). The synthesis of the construct with the appropriate restriction sites was ordered from Twist bioscience. The spike variant was codon optimized for human expression and the construct’s sequence was confirmed by sequencing. Plasmid DNA of the DREP-S vaccine candidate was purified from bacterial cultures using the EndoFree Plasmid Maxi or Giga Kit (QIAGEN) and the concentration and purity was measured on a NanoDrop One (ThermoFisher).

Binding of αCD40.RBD vaccine to non-human primate cells and activation PBMC assays

PBMC from 3 naïve macaques were isolated and stained for 15 min with anti-CD11b-V450 (ICRF44, BD), anti-CD3-V500 (SP34-2, BD), anti-CD11c-BV605 (3.9, BioLegend), anti-CD8-BV650 (BW135/80, Miltenyi Biotec), anti-CD20-SB702 (2H7, Invitrogen), anti-CD163-APC (GHI/61, BioLegend), anti-CD14-A700 (M5E2, BioLegend), anti-HLA-DR-APC-H7 (L243, BD), anti-CD4-FITC (L200, BD), anti-CD45-PerCP (D058-1283, BD)

and anti-CD40-AF594 (12E12) or αCD40.RBD-AF594. Next, cells were washed twice with PBS and acquired on the ZE5 flow cytometer (Biorad). Moreover, a part of these PMBCs were also incubated 18 hours with culture medium (RPMI 1640 media with L-Glutamax supplemented with Penicillin / Streptomycin and 10% of fetal calf serum (FBS)) and stimulated with αCD40.RBD (10 µg/mL) or LPS (100 ng/mL, Invivogen). Next, cells were washed in PBS and incubated 15min with LIVE/DEAD fixable Blue Dead Cell marker (Life Technologies), anti-CD11b-V450 (ICRF44, BD), anti-CD3-V500 (SP34-2, BD), anti-CD86-BV605 (2331, BD), anti-CD11c-APC (3.9, BioLegend), anti-CD20-SB702 (2H7, Invitrogen), anti-CD80-BV786 (L307.4, BD), anti-CD8-BV650 (BW135/80, Miltenyi Biotec), anti-CD14-A700 (M5E2, BioLegend), anti-HLA-DR-APC-H7 (L243, BD), anti-CD4-FITC (L200, BD), anti-CD45-PerCP (D058-1283, BD), anti-CD69-PE-Cy7 (FN50, BD) and anti-CD40-AF594 (42G5). Next, cells were washed twice with PBS and acquired on the ZE5 flow cytometer (Biorad). Analysis was performed on FlowJo v.10 software. For activation markers, results were expressed as fold change geometric MFI, obtained by dividing the geometric MFI measure in αCD40.RBD or LPS stimulation by the background geometric MFI measure in control stimulation (incubation with medium only).

Vaccination of humanized mice

The hu-mice received immunizations at week 0, 3, and 5. The priming injection was an intraperitoneal administration of 10 µg of αCD40-RDB adjuvanted with 50 µg of polyinosinic-polycytidylic acid (Poly-IC; Invivogen) combined or not with an intramuscular injection of DREP-S (10 µg). Then hu-mice received booster i.p injections of αCD40-RDB (10 µg) plus Poly-IC (50 µg). Blood was collected at weeks 0 (before immunization), 3, and 6. Hu-mice were euthanized at week 6.

T-cells response in hu-mice

To analyze the SARS-CoV-2 RBD protein-specific T cell using functional recall assay, we used fifteen-mer peptides (n = 70) overlapping by 11 amino acids (aa) and covering the vaccine RBD sequence (aa281-571 from Spike) synthesized by JPT Peptide Technologies (Berlin, Germany) and used at a final concentration of 1 µg/mL. We also used HLA class I PE labelled tetramers purchased from ProImmune Ltd (Oxford, UK). We used the following two specificities: SARS-CoV-2 A*0201 KIA (KIADYNYKL), SARS-CoV-2 A*0301 KCY (KCYGVSPTK).

Cryopreserved hu-mice spleen cells from 6 weeks after the priming immunization (one week after final immunization) were thawed and counted. Cells were rested overnight in RPMI 1640 media with L-Glutamax supplemented with Penicillin / Streptomycin and 10% of human serum. Subsequently, cells from HLA-A*0201 and HLA-A*0301 donors were pooled together for the mock group and group 2 plus 3 vaccinated hu-mice, then cultured at $0.6x10^6$ cells per condition with 1µg/mL of 15-mers peptides JPT Peptide Technologies (Berlin, Germany). As a negative control no stimulant was added, and as a positive control 1 µL of DynabeadsTM CD3/CD28 (ThermoFischer Scientific) were used. IL-2 (100 IU/mL, R&D System) was added on day 2, half of the volume of each culture well was refreshed with fresh media containing IL-2 (10 U/mL) at day 5 and with fresh media without IL-2 at day 7. On day 8, cells were re-

stimulated: no stimulant was added in the negative control, 100 ng/mL Staphylococcal enterotoxin B (LL-122, Cliniscience) was added in the positive control and 15-mers peptides in the condition of interest. BD GolgiPlug (Becton Dickinson France) was added in all conditions and the culture was continued for additional 18 hours. Next, spleen cells were washed using FACS buffer (PBS, supplemented with 1% FBS) and incubated with tetramer-PE (ProImmune Ltd, Oxford, UK), Live dead fixable Aqua Dead marker (Life Technologies) and the following antibodies: anti-hCD3-A700 (UCHT1, Sony), anti-h-CD4-BV605 (RPA-T4, Sony), anti-hCD8-APC-Cy7 (SK1, Sony) for 30 minutes. Following fixation and permeabilization, spleen cells were stained with intracellular antibodies: anti-hIFNγ-PerCPCy5.5 (B27, Sony), anti-hIL-2-BV421 (17H12, Sony), anti-hTNFα-PC7 (Mab11, Sony) for 30 minutes. Stained cells were acquired on the LSRII flow cytometer (BD Biosciences). FlowJo v.10.7.1 software was used for data analysis (TreeStar, Inc., Ashland, OR).

SARS-CoV-2 S protein-specific B cell analysis

Hu-mice PBMC from 3 weeks after the priming immunization and hu-mice PBMC and spleen cells from 6 weeks (one week after the last recall injection) were incubated first with the biotinylated SARS-CoV-2 S protein for 30 min at 4°C. After a washing step, cells were stained for 30 min at 4°C with streptavine-AF700 (ThermoFisher Scientific), anti-human (h) CD45-PeCy7 (HI30, Sony), anti-mouse (m) CD45-BV711 (30F11, Sony), anti-hCXCR4-Pe-Dazzle (12G5, eBiosciences), anti-hCCR10-PE (314305; R&D System), anti-CD3-FITC (SK7, Biolegend), anti-CD14-FITC (M5E2, Sony), anti-IgM-FITC (MHM-88, Biolegend) antibodies and the following B cell-specific antibodies: anti-hCD19-PacBlue (HIB19, Sony), anti-hCD20-APC (2H7, Sony), anti-hIgG-BV786 (G18-145, BD Biosciences), anti-hCD38-APC-H7 (HIT2, Sony). Staining on spleen cells also included a viability marker (LiveDead aqua or yellow stain ThermoFisher Scientific). Cells were washed twice with FACS buffer (PBS 1% FCS) and acquired on the LSRII flow cytometer (BD Biosciences). Analyses were performed on FlowJo v.10.7.1.

Non-human primate study design

Convalescent cynomolgus macaques previously exposed to SARS-CoV-2 and used to assess hydroxychloroquine (HCQ) and azithromycin (AZTH) antiviral efficacy. None of the AZTH neither HCQ nor the combination of HCQ and AZTH showed a significant effect on viral replication [5]. Six months (24-26 weeks) post infection (p.i.), twelve of these animals were randomly assigned in two experimental groups. The convalescent vaccinated group (n=6) received 200 ug of αCD40.RBD vaccine by subcutaneous (SC) route diluted in PBS and without any adjuvant. The other six convalescent animals were used as controls and received the equivalent volume of PBS by SC. The two groups of convalescent animals were sampled at week 2 and 4 following vaccine or PBS injection for anti-SARS-CoV-2 immune response evaluation. Additional six age matched (43.7 months +/-6.76) cynomolgus macaques from same origin were included in the study as controls naÏve from any exposure to SARS-CoV-2.

Evaluation of anti-Spike, anti-RBD and neutralizing IgG antibodies

Anti-Spike IgG from human and NHP sera were titrated by multiplex bead assay. Briefly, Luminex beads were coupled to the Spike protein as previously described [6] and added to a Bio-Plex plate (BioRad). Beads were washed with PBS 0.05% tween using a magnetic plate washer (MAG2x program) and incubated for 1h with serial diluted individual serum. Beads were then washed and anti-NHP IgG-PE secondary antibody (Southern Biotech, clone SB108a) was added at a 1:500 dilution for 45 min at room temperature. After washing, beads were resuspended in a reading buffer 5 min under agitation (800 rpm) on the plate shaker then read directly on a Luminex Bioplex 200 plate reader (Biorad). Average MFI from the baseline samples were used as reference value for the negative control. Amount of anti-Spike IgG was reported as the MFI signal divided by the mean signal for the negative controls. Human sera from convalescent patients who were hospitalized with virologically confirmed COVID-19 were collected three months after symptoms recovery and used as controls for the titration of anti-Spike antibodies.

Anti-RBD and anti-Nucleocapside (N) IgG were titrated using a commercially available multiplexed immunoassay developed by Mesoscale Discovery (MSD, Rockville, MD) as previously described [7]. Briefly, antigens were spotted at 200–400 µg/mL in a proprietary buffer, washed, dried and packaged for further use (MSD® Coronavirus Plate 2). Then, plates were blocked with MSD Blocker A following which reference standard, controls and samples diluted 1:500 and 1:5000 in diluent buffer were added. After incubation, detection antibody was added (MSD SULFO-TAG™ Anti-Human IgG Antibody) and then MSD GOLD™ Read Buffer B was added and plates read using a MESO QuickPlex SQ 120MM Reader. Results were expressed as arbitrary unit (AU)/mL.

The MSD pseudo-neutralization assay was used to measure antibodies neutralizing the binding of the spike protein to the ACE2 receptor. Plates were blocked and washed as above, assay calibrator (COVID-19 neutralizing antibody; monoclonal antibody against S protein; 200 µg/mL), control sera and test sera samples diluted 1:10 and 1:100 in assay diluent were added to the plates. Following incubation of the plates, an 0.25 µg/mL solution of MSD SULFO-TAG™ conjugated ACE-2 was added after which plates were read as above. Electro-chemioluminescence (ECL) signal was recorded and results expressed as 1/ECL.

Antigen specific T cell assays using non-human primate cells

To analyze the SARS-CoV-2 protein-specific T cell using functional assay, 15-mer peptides (n = 70) overlapping by 11 amino acids (aa) and covering the vaccine RBD sequence (n=70, aa 281-571 from Spike) and the SARS-CoV-2 Nucleoprotein sequence (n=102, aa 1-419 from N) synthesized by JPT Peptide Technologies (Berlin, Germany) and used at a final concentration of 2 µg/mL.

IFNy ELISpot assay of PBMC was performed using the Monkey IFNy ELISpot PRO kit (Mabtech Monkey IFNy ELISPOT pro, #3421M-2APT) according to the manufacturer's instructions. PBMC were stimulated with RBD or N sequence overlapping peptide pools at a final concentration of 2 µg/mL. Plates were incubated for 18 h at 37°C in an atmosphere containing 5% CO2, then washed 5 times with PBS and incubated for 2 h at 37°C with a biotinylated anti-IFNy antibody. After 5 washes, spots were developed by

adding 0.45 µm-filtered ready-to-use BCIP/NBT-plus substrate solution and counted with an automated ELISpot reader ELRIFL04 (Autoimmun Diagnostika GmbH, Strassberg, Germany). Spot forming units (SFU) per 1.0×10^6 PBMC are means of duplicates for each animal.

T-cell responses were also characterized by measurement of the frequency of PBMC expressing IL-2 (PerCP5.5, MQ1-17H12, BD), IL-17a (Alexa700, N49-653, BD), IFN-γ (V450, B27, BD), TNF-α (BV605, Mab11, BioLegend), IL-13 (BV711, JES10-5A2, BD), CD137 (APC, 4B4, BD) and CD154 (FITC, TRAP1, BD) upon stimulation with the two peptide pools. CD3 (APC-Cy7, SP34-2, BD), CD4 (BV510, L200, BD) and CD8 (PE-Vio770, BW135/80, Miltenyi Biotec) antibodies was used as lineage markers. One million of PBMC were cultured in complete medium (RPMI1640 Glutamax+, Gibco; supplemented with 10 % FBS), supplemented with co-stimulatory antibodies (FastImmune CD28/CD49d, Becton Dickinson). Then cells were stimulated with S or N sequence overlapping peptide pools at a final concentration of 2 µg/mL. Brefeldin A was added to each well at a final concentration of 10µg/mL and the plate was incubated at 37°C, 5% CO2 during 18 h. Next, cells were washed, stained with a viability dye (LIVE/DEAD fixable Blue dead cell stain kit, ThermoFisher), and then fixed and permeabilized with the BD Cytofix/Cytoperm reagent. Permeabilized cell samples will be stored at -80 °C before the staining procedure. Antibody staining was performed in a single step following permeabilization. After 30 min of incubation at 4°C, in the dark, cells were washed in BD Perm/Wash buffer then acquired on the ZE5 flow cytometer (Biorad). Analysis was performed on FlowJo v.10 software.

Experimental infection of macaques with SARS-CoV-2

Four weeks after immunization, all animals were exposed to a total dose of 10^6 pfu of SARS-CoV-2 virus (hCoV-19/France/ IDF0372/2020 strain; GISAID EpiCoV platform under accession number EPI_ISL_406596) via the combination of intranasal and intra-tracheal routes (0.25 mL in each nostril and 4.5 mL in the trachea, i.e. a total of 5 mL; day 0), using atropine (0.04 mg/kg) for pre-medication and ketamine (5 mg/kg) with medetomidine (0.05 mg/kg) for anesthesia. Nasopharyngeal, tracheal and rectal swabs, were collected at 1, 2, 3, 4, 6, 9, 14 and 20 days post exposure (d.p.exp.) while blood was taken at 2, 4, 6, 9, 14 and 20 d.p.exp. Bronchoalveolar lavages (BAL) were performed using 50 mL sterile saline at 3 d.p.exp in order to be close to the peak of viral replication and to be able to observe a difference between the vaccinated and control groups. In our earlier study [5], we found that at later time-points, viral loads in the BAL were very low or negative. Chest CT was performed at baseline and at 2 and 6 d.p.exp. on anesthetized animals using tiletamine (4 mg/kg) and zolazepam (4 mg/kg). Lesions were scored as we previously described [5]. Blood cell counts, haemoglobin and haematocrit were determined from EDTA blood using a DXH800 analyzer (Beckman Coulter).

Virus quantification in cynomolgus macaque samples

Upper respiratory (nasopharyngeal and tracheal) and rectal specimens were collected with swabs (Viral Transport Medium, CDC, DSR-052-01). Tracheal swabs were performed by insertion of the swab above the tip of the epiglottis into the upper trachea at approximately 1.5 cm of the epiglottis. All specimens

were stored between 2°C and 8°C until analysis by RT-qPCR with a plasmid standard concentration range containing an RdRp gene fragment including the RdRp-IP4 RT-PCR target sequence. The limit of detection was estimated to be 2.67 $\log_{10}$ copies of SARS-CoV-2 gRNA per mL and the limit of quantification was estimated to be 3.67 $\log_{10}$ copies per mL. SARS-CoV-2 E gene subgenomic mRNA (sgRNA) levels were assessed by RT-qPCR using primers and probes previously described (Corman et al., 2020; Wölfel et al., 2020): leader-specific primer sgLeadSARSCoV2-F CGATCTCTTGTAGATCTGTTCTC, E-Sarbeco-R primer ATATTGCAGCAGTACGCACACA and E-Sarbeco probe HEX-ACACTAGCCATCCTTACTGCGCTTCG-BHQ1. The protocol describing the procedure for the detection of SARS-CoV-2 is available on the WHO website (https://www.who.int/docs/default-source/coronaviruse/real-time-rt-pcr-assays-for-the-detection-of-sars-cov-2-institut-pasteur-paris.pdf?sfvrsn=3662fcb6_2). The limit of detection was estimated to be 2.87 $\log_{10}$ copies of SARS-CoV-2 sgRNA per mL and the limit of quantification was estimated to be 3.87 $\log_{10}$ copies per mL.

Viral dynamics modeling

For the structure of the model, we started from previously published models [8,9] where we added a compartment for the inoculum to be able to distinguish between the injected virus (V_s) and the virus produced de novo (V_I and V_{NI}). The model included uninfected target cells (T) that can be infected (I_1) and produce virus after an eclipse phase (I_2). The virus generated can be infectious (V_I) or non infectious (V_{NI}). The model can be written as a set of differential equations as follows:

$$\begin{aligned}
\frac{dT}{dt} &= -\beta V_I T - \mu\beta V_S T \\
\frac{dI_1}{dt} &= \beta V_I T + \mu\beta V_S T - kI_1 \\
\frac{dI_2}{dt} &= kI_1 - \delta I_2 \\
\frac{dV_I}{dt} &= \mu p I_2 - cV_I - \beta V_I T \\
\frac{dV_{NI}}{dt} &= (1-\mu) p I_2 - cV_{NI} \\
\frac{dV_S}{dt} &= -cV_S - \mu\beta V_S T
\end{aligned}$$

Using the concentration of viral load, measuring V_S, V_I and V_{NI}, we estimated the viral infectivity (β) and the loss rate of infected cells (δ). The effect of each intervention group (convalescent macaques vaccinated or not and previously uninfected macaques) was tested on the viral infectivity and the loss rate of infected cells. Furthermore, individual variation of β, ρ and δ was estimated through random effects. Maximum likelihood estimation was performed using a stochastic approximation EM algorithm

implemented in the software Monolix (www.lixoft.com). The duration of the eclipse phase ($1/\kappa$) and the clearance of the virus (c) were estimated by profile likelihood. The production of viral particles by infected cells (ρ) has been fixed to 19,000 in trachea and 36,000 in nasopharynx copies per productively infected cell per day according to previous estimations [5]. The proportion of infectious virus (m) has been fixed to 1/1000 according to previous work [5]. The initial concentration of target cells, that are the epithelial cells expressing the ACE2 receptor, was assumed to be 1.33×10^5 cells/mL in the nasopharynx and 2.25×10^4 cells/mL in trachea (Gonçalves et al., 2020). The initial concentration of the inoculum was assumed to be 2.3×10^9 copies/mL corresponding to 10^6 pfu (Table 1).

Table 1. Model parameters for viral dynamics in the trachea. Infection rates (β) and loss rates of infected cells (δ) were estimated by the direct maximum-likelihood approach. The eclipse rate (k) and viral clearance (c) were estimated by the profile likelihood, exploring various potential values for c (1,5,10,15,20,30) and k (1, 3, 6).

Parameter	Meaning	Value [95% Confidence interval]	Unit
β	Infection rate in the naive & non-vaccinated	$2.9x10^{-3}$ [$1.2x10^{-3}$; $6.7x10^{-3}$]	$day{-}1.virions{-}1$
	Convalescent groups		
	Fold change in the vaccine group	0.01 [0.00; 0.07]*	
	αCD40.RBD vaccine blockade of new infections	99% [70%;100%]	
k	Eclipse rate	3	$day{-}1$
δ	Loss rate of infected cells in the naive group	0.94 [0.87 ; 1.02] $day{-}1$	
	Fold change in the convalescent group	2.18 [1.90 ; 2.49]*	
	Percentage increase of infected cell death in non-vaccinated convalescents vs naive animals	118%	
	Fold change in the vaccine group	2.86 [2.13 ; 3.81]*	
	Percentage increase of infected cell death in vaccinated vs convalescent animals	31%	
	Percentage increase of infected cell death in vaccinated vs naive animals	149%	
μ	Percentage of infectious viruses	0.001	$day{-}1$
p	Viral production	19000	$day{-}1$
c	Viral clearance	20	$day{-}1$
T_0	Initial concentration of target cells	$2.25x10^4$	$cells.mL{-}1$
V_{S0}	Initial concentration of inoculum (sRNA)	$4.3x10^9$	$copies.mL{-}1$

*P < 0.001, Wald test for fold change different from 1.

Statistical analysis

Differences between unmatched groups were compared using an unpaired t-test or the Mann-Whitney U test (Graphpad Prism 8.0), and differences between matched groups were compared using a paired t-test or the Wilcoxon signed-rank test (Graphpad Prism 8.0). Viral kinetic parameter was compared using log-rank tests (Graphpad Prism 8.0). Correlation between viral and immune parameter was determined using nonparametric Spearman correlation (Graphpad Prism 8.0).

Declarations

ACKNOWLEDGEMENTS

We thank B. Delache, S. Langlois, J. Demilly, N. Dhooge, P. Le Calvez, M. Potier, J. M. Robert, T. Prot and C. Dodan for the NHP experiments; L. Bossevot, M. Leonec, L. Moenne-Loccoz, M. Calpin-Lebreau and J. Morin for the RT-qPCR, ELISpot and Luminex assays, and for the preparation of reagents; W. Gros for NHP T-cell assays and flow cytometry; B. Fert for her help with the CT scans; S. Tricot for fluorescent labelling of Ab used in flow cytometry; M. Barendji, J. Dinh and E. Guyon for the NHP sample processing; S. Keyser for the transports organization; F. Ducancel and Y. Gorin for their help with the logistics and safety management; I. Mangeot for here help with resources management and B. Targat contributed to data management; We thank S. Bellil and V. Enouf for contribution to viral stock challenge production and A. Nougairede for sharing the plasmid used for the sgRNA assays standardization.

Funding: The programme was funded by the Vaccine Research Institute via the ANR-10-LABX-77 grant. Studies in hu-mice model have been supported by ARN grant ANR-20-COV6-0004-01. The Infectious Disease Models and Innovative Therapies (IDMIT) research infrastructure is supported by the 'Programme Investissements d'Avenir, managed by the ANR under reference ANR-11-INBS-0008. The Fondation Bettencourt Schueller and the Region Ile-de-France contributed to the implementation of IDMIT's facilities and imaging technologies. The NHP study received financial support from REACTing, the Fondation pour la Recherche Medicale (FRM; AM-CoV-Path) and the European Infrastructure TRANSVAC2 (730964) for implementation of in vivo imaging technologies an NHP immune assays. the Fondation Bettencourt Schueller and the Region Ile-de-France for the contribution to the implementation of imaging facilities; and the Domaine d'Intérêt Majeur (DIM) 'One Health' for its support. The NHP model of SARS-CoV-2 infection was developed thanks to the help of REACTing (Paris france), the National Research Agency (ANR, Paris, france; AM-CoV-Path) and the European Union's Horizon 2020 (H2020) research and innovation program Fight-nCov (101003555), European Union IMI2 program CARE (101005077) and the European Infrastructure TRANSVAC2 (730964). The virus stock was obtained through the EVAg platform (https://www.european-virus-archive.com/), funded by H2020 (653316).

Author contributions: Y.L., G.Z. and R.L.G. Conceptualization, study design, supervision, data analysis, project administration and writing. R.M., M.G., V.G. and S.C: Methodology, validation, formal analysis, data curation, figures elaboration Writing - Original Draft, Visualization; R.M. and M.C: project administration. S.Z, Z.W., Y.L., J.E: Design and production of αCD4.RBD vaccines; N.D.B.: development of viral load assays and analysis, T cell assays project administration; A.S.G., M.G.P.: Supervision, T cell analysis and flow cytometry; S.C, C.F, G.P, M.C.: serology assays in NHP and analysis; J.L, F.R, R.H.S.F., L.D.: animal studies; T.N, N.K: in vivo imaging and CT analysis. S.V.D.W.: viral stock production and characterization, data analysis

Competing interest: The funders had no role in study design, data collection, data analysis, data interpretation, or data reporting.

Disclosures

The authors S.Z., G.Z., V.G., M.C. and Y.L, are named inventors on patent applications based on this work held by Inserm Transfert.

Data and materials availability: All data are available in the manuscript or the supplementary material.

References

1. M. Voysey *et al.*, Safety and efficacy of the ChAdOx1 nCoV-19 vaccine (AZD1222) against SARS-CoV-2: an interim analysis of four randomised controlled trials in Brazil, South Africa, and the UK. *Lancet (London, England)*, (2020).
2. K. S. Corbett *et al.*, Evaluation of the mRNA-1273 Vaccine against SARS-CoV-2 in Nonhuman Primates. *N Engl J Med* **383**, 1544-1555 (2020).
3. F. P. Polack *et al.*, Safety and Efficacy of the BNT162b2 mRNA Covid-19 Vaccine. *N Engl J Med*, (2020).
4. N. B. Mercado *et al.*, Single-shot Ad26 vaccine protects against SARS-CoV-2 in rhesus macaques. *Nature* **586**, 583-588 (2020).
5. S. E. Oliver *et al.*, The Advisory Committee on Immunization Practices' Interim Recommendation for Use of Pfizer-BioNTech COVID-19 Vaccine - United States, December 2020. *MMWR Morb Mortal Wkly Rep* **69**, 1922-1924 (2020).
6. A. T. Widge *et al.*, Durability of Responses after SARS-CoV-2 mRNA-1273 Vaccination. *N Engl J Med*, (2020).
7. E. J. Anderson *et al.*, Safety and Immunogenicity of SARS-CoV-2 mRNA-1273 Vaccine in Older Adults. *N Engl J Med* **383**, 2427-2438 (2020).
8. J. T. Schiller, D. R. Lowy, Raising expectations for subunit vaccine. *J Infect Dis* **211**, 1373-1375 (2015).
9. X. Ma *et al.*, Nanoparticle Vaccines Based on the Receptor Binding Domain (RBD) and Heptad Repeat (HR) of SARS-CoV-2 Elicit Robust Protective Immune Responses. *Immunity* **53**, 1315-1330.e1319 (2020).
10. P. J. M. Brouwer *et al.*, Two-component spike nanoparticle vaccine protects macaques from SARS-CoV-2 infection. *bioRxiv*, 2020.2011.2007.365726 (2020).
11. K. McMahan *et al.*, Correlates of protection against SARS-CoV-2 in rhesus macaques. *Nature*, (2020).
12. W. Yin *et al.*, Functional Specialty of CD40 and Dendritic Cell Surface Lectins for Exogenous Antigen Presentation to CD8(+) and CD4(+) T Cells. *EBioMedicine* **5**, 46-58 (2016).
13. V. Godot *et al.*, TLR-9 agonist and CD40-targeting vaccination induces HIV-1 envelope-specific B cells with a diversified immunoglobulin repertoire in humanized mice. *PLoS pathogens* **16**, e1009025

(2020).

14. L. Cheng *et al.*, TLR3 agonist and CD40-targeting vaccination induces immune responses and reduces HIV-1 reservoirs. *J Clin Invest* **128**, 4387-4396 (2018).
15. A. Bouteau *et al.*, DC Subsets Regulate Humoral Immune Responses by Supporting the Differentiation of Distinct Tfh Cells. *Frontiers in immunology* **10**, 1134 (2019).
16. G. Zurawski *et al.*, Superiority in Rhesus Macaques of Targeting HIV-1 Env gp140 to CD40 versus LOX-1 in Combination with Replication-Competent NYVAC-KC for Induction of Env-Specific Antibody and T Cell Responses. *Journal of virology* **91**, (2017).
17. J. Shang *et al.*, Cell entry mechanisms of SARS-CoV-2. *Proc Natl Acad Sci U S A* **117**, 11727-11734 (2020).
18. A. L. Flamar *et al.*, Targeting concatenated HIV antigens to human CD40 expands a broad repertoire of multifunctional CD4+ and CD8+ T cells. *Aids* **27**, 2041-2051 (2013).
19. A. L. Flamar *et al.*, Noncovalent assembly of anti-dendritic cell antibodies and antigens for evoking immune responses in vitro and in vivo. *Journal of immunology (Baltimore, Md. : 1950)* **189**, 2645-2655 (2012).
20. I. Szurgot *et al.*, DNA-launched RNA replicon vaccines induce potent anti-SARS-CoV-2 immune responses in mice. *Scientific Reports*, (2021).
21. K. Ljungberg, P. Liljeström, Self-replicating alphavirus RNA vaccines. *Expert Rev Vaccines* **14**, 177-194 (2015).
22. E. Klechevsky *et al.*, Cross-priming CD8+ T cells by targeting antigens to human dendritic cells through DCIR. *Blood* **116**, 1685-1697 (2010).
23. P. Maisonnasse *et al.*, Hydroxychloroquine use against SARS-CoV-2 infection in non-human primates. *Nature*, (2020).
24. C. Gaebler *et al.*, Evolution of Antibody Immunity to SARS-CoV-2. *bioRxiv*, (2020).
25. P. Baccam, C. Beauchemin, C. A. Macken, F. G. Hayden, A. S. Perelson, Kinetics of influenza A virus infection in humans. *Journal of virology* **80**, 7590-7599 (2006).
26. A. Gonçalves *et al.*, Timing of Antiviral Treatment Initiation is Critical to Reduce SARS-CoV-2 Viral Load. *CPT Pharmacometrics Syst Pharmacol* **9**, 509-514 (2020).
27. J. I. Cohen, P. D. Burbelo, Reinfection with SARS-CoV-2: Implications for Vaccines. *Clin Infect Dis*, (2020).
28. J. Seow *et al.*, Longitudinal observation and decline of neutralizing antibody responses in the three months following SARS-CoV-2 infection in humans. *Nat Microbiol* **5**, 1598-1607 (2020).
29. A. Chandrashekar *et al.*, SARS-CoV-2 infection protects against rechallenge in rhesus macaques. *Science* **369**, 812-817 (2020).

Methods references

1. Flamar, A. L. *et al.* Targeting concatenated HIV antigens to human CD40 expands a broad repertoire of multifunctional CD4+ and CD8+ T cells. *Aids* **27**, 2041-2051, doi:10.1097/QAD.0b013e3283624305 (2013).
2. Li, D. *et al.* Targeting self- and foreign antigens to dendritic cells via DC-ASGPR generates IL-10-producing suppressive CD4+ T cells. *J Exp Med* **209**, 109-121, doi:10.1084/jem.20110399 (2012).
3. Zurawski, G. *et al.* Superiority in Rhesus Macaques of Targeting HIV-1 Env gp140 to CD40 versus LOX-1 in Combination with Replication-Competent NYVAC-KC for Induction of Env-Specific Antibody and T Cell Responses. *Journal of virology* **91**, doi:10.1128/jvi.01596-16 (2017).
4. Szurgot, I. *et al.* DNA-launched RNA replicon vaccines induce potent anti-SARS-CoV-2 immune responses in mice. *Scientific Reports* (2021).
5. Maisonnasse, P. *et al.* Hydroxychloroquine use against SARS-CoV-2 infection in non-human primates. *Nature*, doi:10.1038/s41586-020-2558-4 (2020).
6. Fenwick, C. *et al.* Changes in SARS-CoV-2 Spike versus Nucleoprotein Antibody Responses Impact the Estimates of Infections in Population-Based Seroprevalence Studies. *Journal of virology* **95**, doi:10.1128/jvi.01828-20 (2021).
7. Johnson, M. *et al.* Evaluation of a novel multiplexed assay for determining IgG levels and functional activity to SARS-CoV-2. *J Clin Virol* **130**, 104572, doi:10.1016/j.jcv.2020.104572 (2020).
8. Baccam, P., Beauchemin, C., Macken, C. A., Hayden, F. G. & Perelson, A. S. Kinetics of influenza A virus infection in humans. *Journal of virology* **80**, 7590-7599, doi:10.1128/jvi.01623-05 (2006).
9. Gonçalves, A. *et al.* Timing of Antiviral Treatment Initiation is Critical to Reduce SARS-CoV-2 Viral Load. *CPT Pharmacometrics Syst Pharmacol* **9**, 509-514, doi:10.1002/psp4.12543 (2020)

Figures

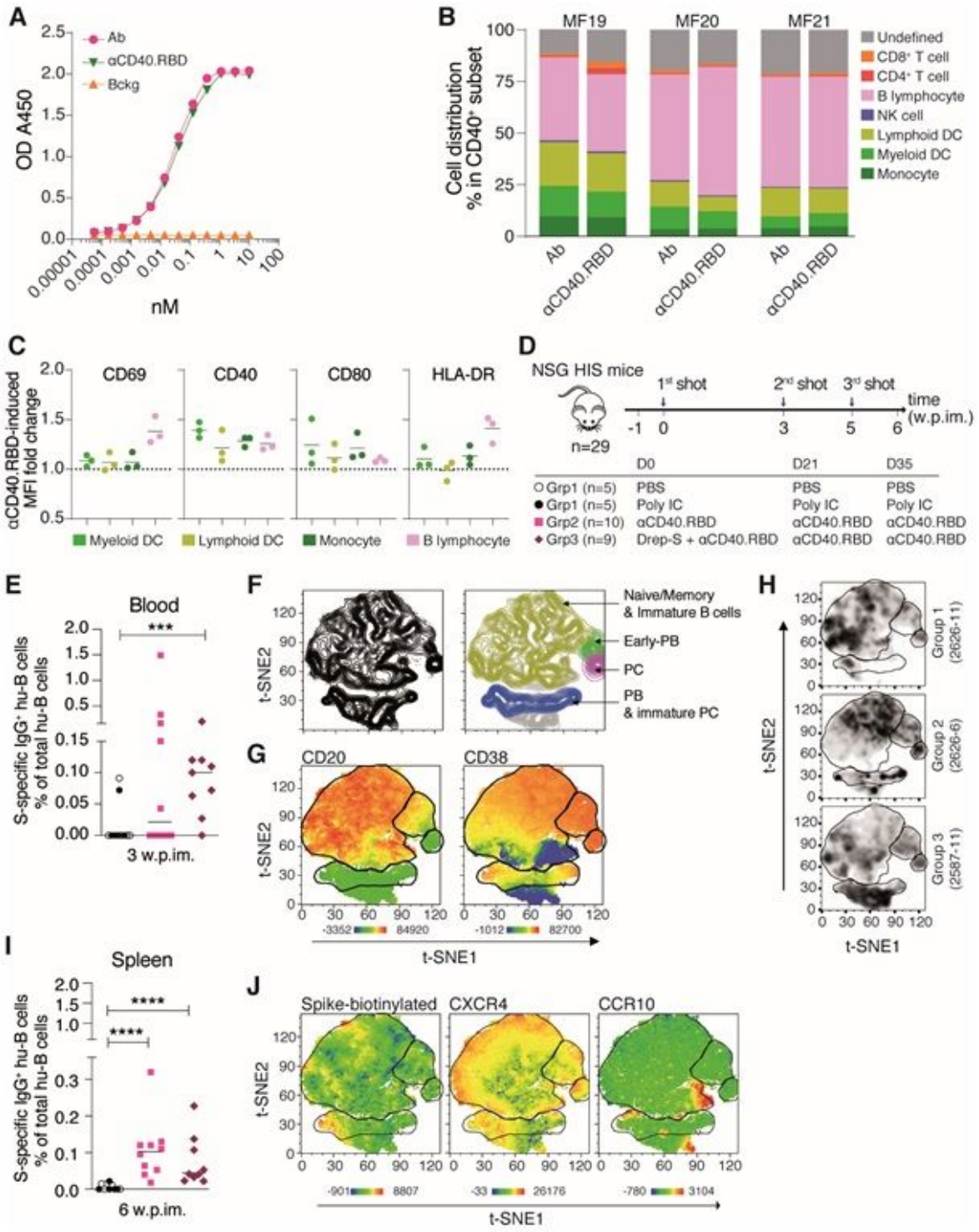

Figure 1

αCD40.RBD vaccine targeting and immunogenicity in hu-mice. (A) Binding to solid-phase attached human CD40 ectodomain protein by anti-CD40 12E12 human monoclonal antibody (Ab, filled pink circles) by the anti-CD40 12E12-RBD vaccine (αCD40.RBD, filled green triangles) and control IgG4 (bckg, filled orange triangles). (B) Binding of 12E12 antibody (Ab) and αCD40.RBD vaccine to CD40-expressing PBMCs of three naive cynomolgus macaques measured by flow cytometry. Cell subsets were defined by

the gating strategy shown in Extended data Fig. 1B. (C) Fold change of the geometric mean fluorescence intensity (MFI) of activation markers after 18 h of incubating NHP (n = 3) PBMCs with the αCD40.RBD vaccine for cell subsets targeted by the αCD40.RBD vaccine and identified in (B). (D) Schematic overview of vaccination strategies in NSG humanized (hu) mice, including three experimental groups, 9 to 10 animals/group. (E) SARS-CoV-2 S protein-specific IgG-switched human B-cell frequencies within the hu-B cells in the blood of hu-mice three weeks after the priming injection. (F) Flow cytometry t-SNE analysis of splenic CD19+ B cells based on five markers (mCD45, hCD45, hCD19, hCD20, hCD38) showing the clustering of PCs, early plasma blasts (PBs), and a population of PBs and immature PCs. (G) Mapping of CD20 and CD38 onto the splenic hu-B-cell clusters obtained following t-SNE analysis. (H) Representative examples of t-SNE of one hu-mouse from each group. (I) SARS-CoV-2 S protein-specific IgG-switched human B-cell frequencies within the hu-B cells in the spleen of hu-mice six weeks after the priming injection. (J) Mapping of the SARS-CoV-2 S protein trimer, CXCR4, and CCR10 onto the splenic hu-B-cell clusters obtained following t-SNE analysis.

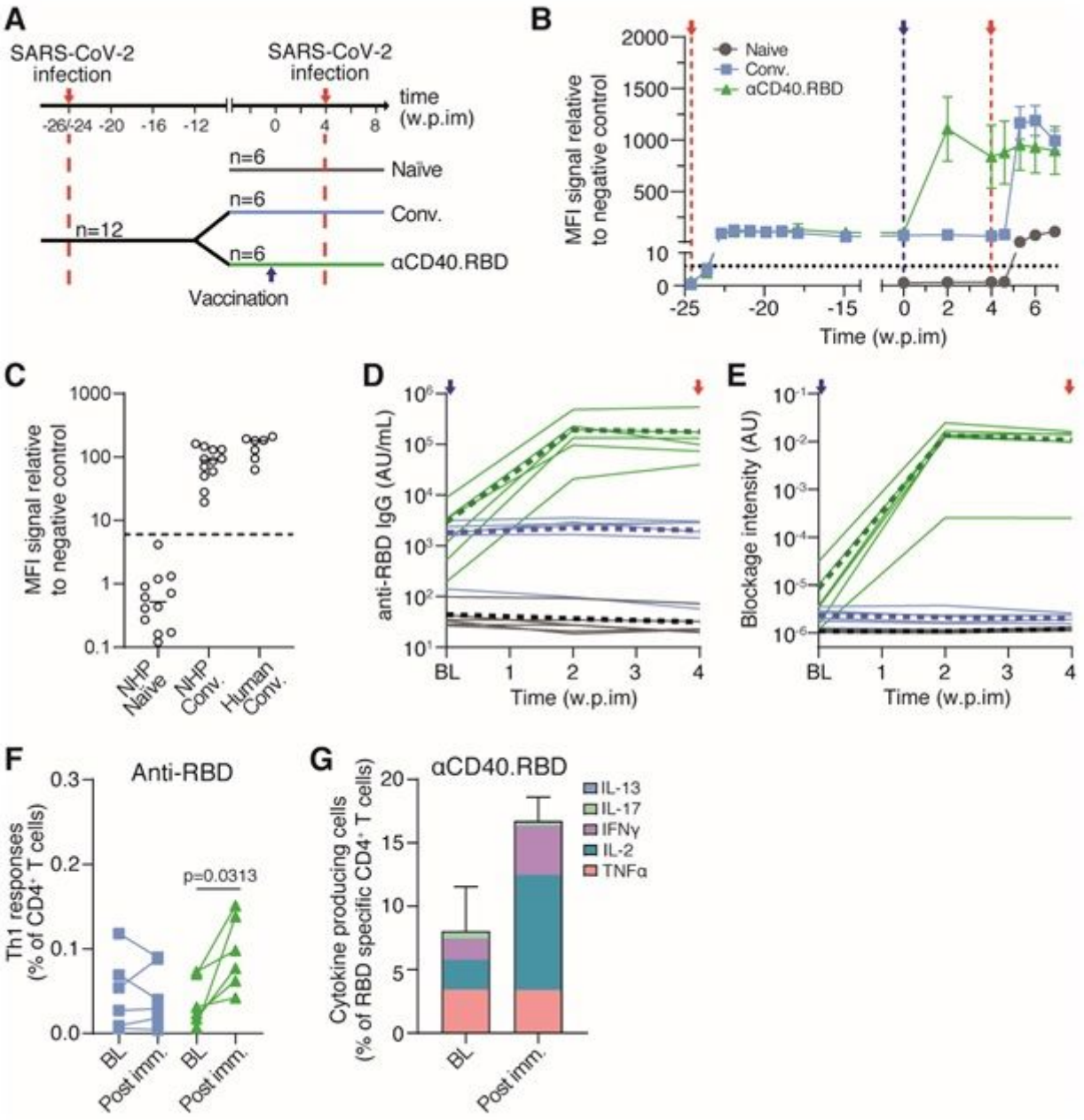

Figure 2

SARS-CoV-2 specific B- and T-cell responses induced by αCD40.RBD in convalescent NHP. (A) Study design in cynomolgus macaques. (B) Relative MFI of IgG binding to SARS-CoV-2 S protein, measured using a Luminex-based serology assay, in serum samples (mean ± SD of 6 animals per group). The red and blue vertical dotted lines indicate viral exposure and vaccination, respectively. (C) SARS-CoV-2 S protein-specific binding before any exposure to SARS-CoV-2 (week -26) and on the week of vaccine injection (week 0) in macaques (n = 12) compared to convalescent humans (n = 7) sampled 24 weeks after the onset of symptoms. The horizontal dotted line represents the background threshold. (D) Quantification of SARS-CoV-2 antibodies against RBD measured in the serum of NHPs using a multiplexed solid-phase chemiluminescence assay. Each plain line indicates the individual values, and

the bold dotted lines represent the mean for each experimental group. (E) Quantification of antibody-induced inhibition of ACE-2 binding in NHP serum. Symbols are as for panel D. (F) Frequency of RBD-specific Th1 CD4+ T cells (CD154+ and IFN-+/- IL-2+/- TNF-α) in the total CD4+ T cell population for each non-immunized convalescent macaque (blue lines and symbols) and αCD40.RBD-vaccinated convalescent macaque (green lines and symbols). PBMC were stimulated overnight with SARS-CoV-2 RBD overlapping peptide pools. Time points in each experimental group were compared using the Wilcoxon signed rank test. (G) Frequency of cytokine producing cells in the RBD-specific CD4+ T cells (CD154+) for αCD40.RBD-vaccinated convalescent macaque. Each bar indicated the mean of the 6 vaccinated convalescent macaques. Distribution of cytokines is indicated within each bar. BL: Baseline approximately 1 week before immunization; “Post imm.”: Two weeks post immunization.

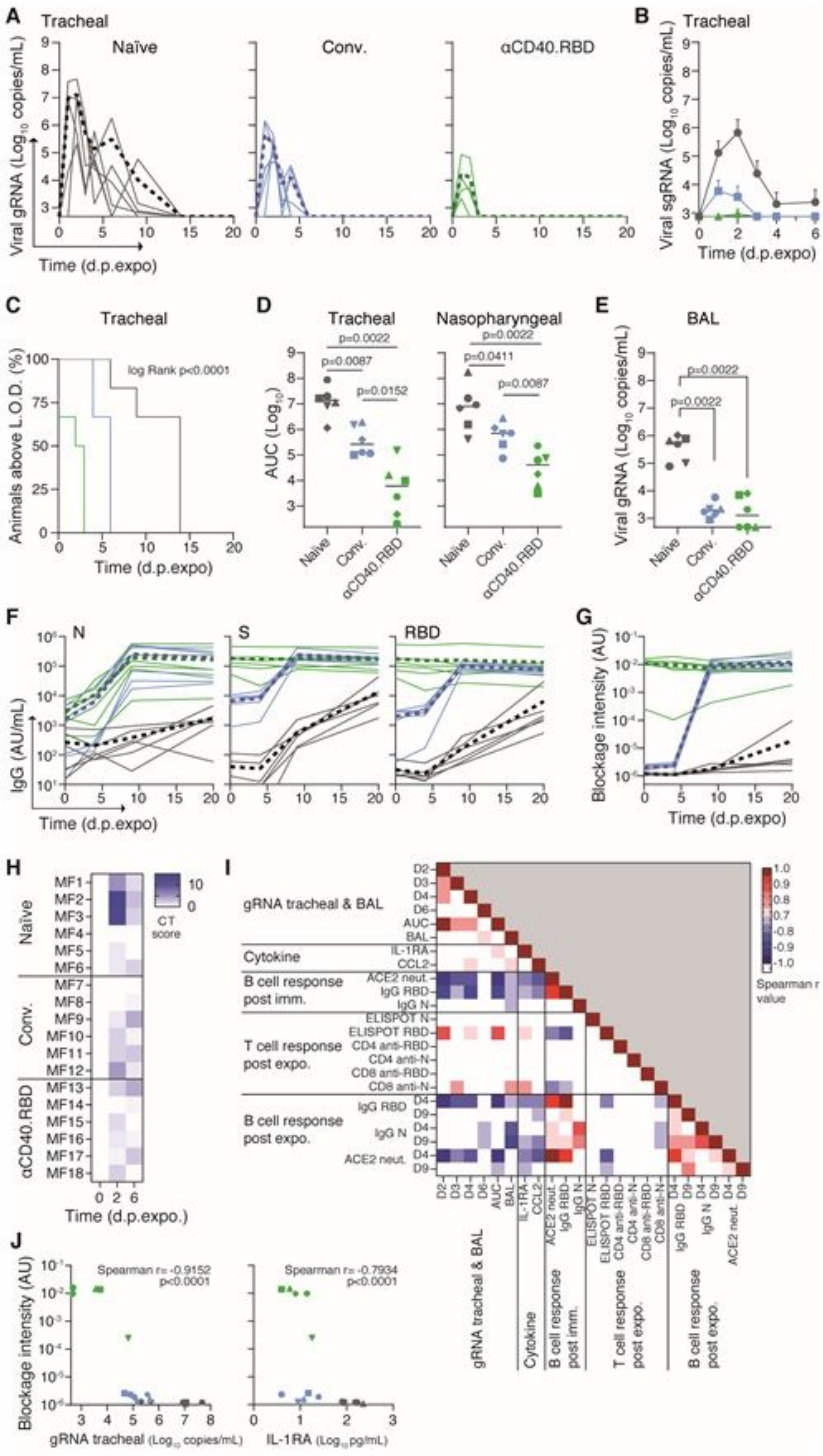

Figure 3

Efficacy of αCD40.RBD in convalescent cynomolgus macaques. (A) Genomic viral RNA (gRNA) quantification in tracheal swabs of naive (left, grey lines), convalescent (middle, blue lines), and αCD40.RBD-vaccinated convalescent macaques (right, green lines). The bold line represents the mean viral load for each experimental group. (B) Mean of subgenomic (sgRNA) viral loads in tracheal swabs. (C) Percentage of macaques with viral gRNA above the limit of detection (LOD) over time in tracheal

swabs. Experimental groups were compared using log Rank tests. (D) Area under the curve (AUC) of gRNA viral loads in tracheal (left panel) and nasopharyngeal swabs (right panel). (E) gRNA viral quantification in BAL three days post-exposure (d.p.expo). Groups were compared using the non-parametric Mann-Whitney test. (F) Quantification of SARS-CoV-2 IgG binding N, S, and RBD after challenge. Each plain line indicates individual values, and the bold dotted lines represent the mean for each experimental group. (G) Quantification of antibody-induced inhibition of ACE-2 binding. Lines as in panel F. (H) Lung CT-scores of macaques before challenge and at 2 and 6 d.p.expo to SARS-CoV-2. The CT score includes lesion type and lesion volume summed for each lobe. (I) Correlation matrix between virological and immune parameters. The heatmap indicates the Spearman r values (Only values between -0.7 and -1, and 0.7 and 1 are colored in the heatmap). (J) Correlation between antibody-induced inhibition of ACE-2 binding at 0 d.p.expo. and tracheal gRNA viral loads (left) or IL-1RA plasma concentration (right) at 2 d.p.expo.

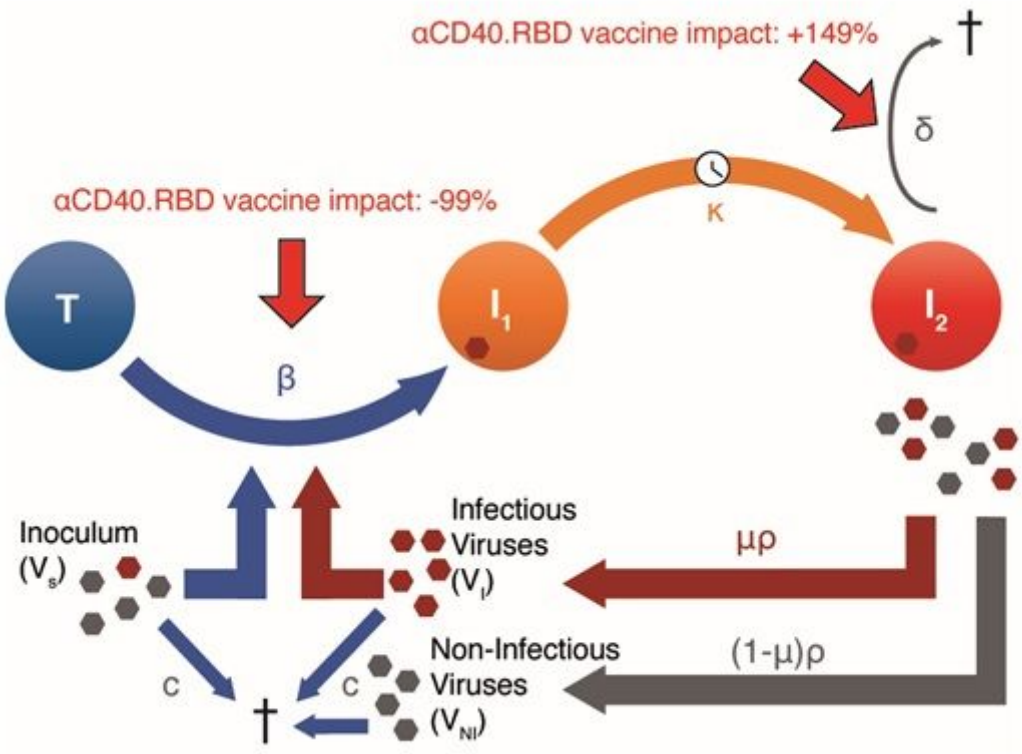

Figure 4

Modeling of viral dynamics. Estimations of the effect of the αCD40.RBD-vaccinated convalescent group on the infectivity (β) and clearance of the infected cells (δ) in the trachea relative to naïve control group. T: uninfected target cells, I1: Infected cells, I2: productively-infected cells, Vs: Virus inoculum, grey hexagon: non-infectious viral particles (VNI), Red hexagon: infectious viral particles (VI).

Supplementary Files

This is a list of supplementary files associated with this preprint. Click to download.

- ExtendedDataFigures.pdf